Engineered Science
DOI: https://dx.doi.org/10.30919/es1226

Influence of the Oxide Film on the Performance and Corrosion Resistance of TiNiCu Shape Memory Alloys as the Heat Engine Actuator

Aphinan Phukaoluan,[1,*] Kasama Srirussamee,[2] Anak Khantachawana,[3,4] Monthon Chuchonak[1] and Phacharaphon Tunthawiroon[5]

Abstract

Shape memory alloys (SMAs) are utilized as an actuator for the heat engine to harvest energy from low-temperature geothermal sources, such as hot springs, which convert thermal energy into mechanical work. However, the alloy processing and engine design still require optimization to improve performance and durability. To discuss their potential as heat engine actuator, this study investigated the influence of oxide films on the TiNiCu SMAs in terms of surface and structural properties, recovery forces, and corrosion resistance. The results show that the surfaces of the etched samples were relatively coarser than those unetched with lower oxygen content. With the presence of oxide film, the Austenite Finish Temperature (A_f) temperature of the unetched SMAs was lower with R-phase transformation. Also, it provided higher recovery force at above A_f temperature (as high as 8.3 N at 70-mm displacement). Furthermore, the corrosion resistance of the unetched SMAs was higher than the etched samples, as analyzed by open-circuit potential and linear polarization in natural spring water at 70°C. These findings imply that the presence of oxide film could be beneficial for the SMAs when used as an actuator for heat engines, although it may require further study to investigate its impact on the fatigue behavior of the alloys.

Keywords: Shape memory alloys; Heat engine; Oxide formation; Corrosion resistance.
Received: 28 June 2024; Revised: 21 August 2024; Accepted: 06 September 2024.
Article type: Research article.

1. Introduction

Global warming has emerged as one of the major crises nowadays. The rise in average temperature was attributed to the release of greenhouse gases, particularly from fossil fuel consumption. As a result, alternative approaches have been implemented to mitigate this issue, including the use of solar or geothermal energy.[1] However, the efficiency of these approaches is also dependent on the condition of the sources, such as the accessible sunlight or the temperature of geothermal sources. Despite abundant availability, hot springs, one of the most commonly accessible geothermal energy sources across over 80 countries, are regarded as low-grade heat sources due to their low temperature ranging between 21 and 149 °C.[2,3] Besides, this temperature range is also generally considered as low-efficiency for energy harvest.[3]

During the past few decades, several attempts have been made to harvest heat from low-temperature sources,[4-7] one of which is the use of shape memory alloy (SMA) heat engine.[8] This approach is based on the thermoelastic properties of SMAs, which undergo phase changes between B19' monoclinic (martensite) and B2 cubic (austenite) influenced by temperature changes, resulting in force and displacement generation.[9-11] As a result, SMAs are used as actuators for several heat engine designs, which have been demonstrated to successfully convert heat to mechanical work at various power densities and efficiencies.[9,12,13] Nonetheless, the durability of

[1] *Department of Mechanical and Industrial Engineering, Faculty of Engineering, Rajamangala University of Technology Krungthep, Bangkok 10120, Thailand.*
[2] *Department of Biomedical Engineering, School of Engineering, King Mongkut's Institute of Technology Ladkrabang, Bangkok 10520, Thailand.*
[3] *Department of Mechanical Engineering, Faculty of Engineering, King Mongkut's University of Technology Thonburi, Bangkok 10140, Thailand.*
[4] *Biological Engineering Program, Faculty of Engineering, King Mongkut's University of Technology Thonburi, Bangkok 10140, Thailand.*
[5] *Department of Industrial Engineering, School of Engineering, King Mongkut's Institute of Technology Ladkrabang, Bangkok 10520, Thailand.*
**Email:* aphinan.p@mail.rmutk.ac.th (A. Phukaoluan)

the SMA heat engine may also require further optimization as a number of cyclic deformations are taking place during the operation that could lead to fatigue.[14] Moreover, material degradation could also occur when SMAs are exposed to the environment, potentially affecting their force and displacement generation.

Common types of SMAs are TiNi-based, which are known for their excellent corrosion resistance. This is primarily due to the stability of the oxide films and interfaces formed on the surface of the alloys. In some cases, these oxide layers also affect phase transformation, such as the presence of the rhombohedral phase (R-phase).[15] Moreover, some alloying elements, such as Cu, have also been introduced to improve the structural properties of TiNi-based alloys. In general, thin and smooth oxide layers are formed on the surface of TiNi-based alloys through oxidation below 500 °C[16] and become thick and porous at above 600°C with other interfacial layers, including TiO_2 and Ti-Ni intermetallic compounds.[16-20] These layers are formed by atomic diffusion and the oxidation reaction at the surface. As a result, localized changes in the alloy composition are possible, depending on the heat treatment composition.[21,22] Furthermore, it has also been shown that oxide formation layers on the TiNi alloys could increase the stress required to induce martensitic transformation, strength and hardness; nonetheless, the excessive oxide formation could significantly reduce the ductility.[21,23,24] It could be seen that properties of SMAs can be manipulated through surface oxidation; however, the limited number of studies has demonstrated and discussed whether or not the presence of the oxide layers is beneficial for the application of SMAs as the heat engine actuator in terms of performance and durability.[25]

Furthermore, excessive oxide formation could also be regarded as a surface imperfection affecting materials properties and may be removed for aesthetic reasons. Therefore, this study aims to investigate the influence of oxide films on the performance of TiNiCu SMAs as the heat engine actuator and their corrosion resistance when exposed to natural spring water. Forces generated by the alloys and the corresponding displacement are measured and discussed alongside surface and corrosion resistance characterization. In addition, the offset crankshaft mechanism is also used for the pilot test. It is expected the findings from this study will provide beneficial information for the SMA heat engine design in the future.

2. Materials and methods

2.1 TiNiCu shape memory alloys (SMAs)

SMA wires with a diameter of 0.7 mm (NT-H8 As-Drawn, Furukawa Techno Material) were used in this study. These wires were shaped into a helical spring-like structure with an inner spring diameter of 4 mm (spring index of 6.71).[26] The shaped wires underwent two different annealing treatment conditions: one at 350 °C for 30 minutes; and another for 60 minutes. Following the annealing process, the wires were promptly quenched in ice-cold water. Finally, the etching process was carried out by immersing in a mixture of 48% hydrofluoric acid (LobaChemie), 70% nitric acid (UNIVAR®, Ajax Finechem), and distilled water (volume ratio of 1:4:5) followed by washing in distilled water and methanol, respectively. The duration of the etching process was controlled at approximately 1 minute to remove the oxide layers of a specific set of samples and avoid significant effects on the underlying layer.

2.2 Surface characterization and profile measurement

The surface of the samples was characterized using 3D confocal laser microscope (OLYMPUS LEXT OLS5000-SAF). Laser images were taken at 20X magnification, from which the corresponding transverse profiles were measured using the 'manufacturer's software.

2.3 Scanning electron microscope and energy dispersive X-Ray spectroscopy (SEM-EDS)

A cross-section of the samples was sputter coated with gold and examined using SEM at a magnification of 5,000X with 20 kV accelerating voltage (Apreo S, ThermoFisher Scientific). Relative chemical compositions across the depth from the outer layer were qualitatively analyzed using energy dispersive X-ray spectroscope (EDS) (Ultim® Max, Oxford Instruments) line scan at 10,000X magnification, including Ti, Ni, Cu, and O.

2.4 Differential scanning calorimetry (DSC)

Differential scanning calorimetry (DSC) was used to analyze the samples' phase transformation temperatures (METTLER TOLEDO, DSC-1) by measuring thermal changes within the specific temperature range. Samples were heated from room temperature (RT) to 100 °C and cooled down to 0 °C before being heated again to 100 °C. The heating and cooling rate was set at 10 °C/min.[27] Martensite start (M_s) and finish (M_f) transformation temperatures were determined using the extrapolated tangential method from the peaks during the cooling cycle. On the other hand, Austenite start (A_s) and (A_f) transformation temperatures were determined from the second heating cycle.

2.5 Recovery force measurement

A universal tensile testing machine equipped with 100-N load cell (MultiTest 2.5-i, Mecmesin) was used to measure force and displacement generated by the SMA springs. The test was conducted at 5 mm/min speed up to the total displacement of 70 mm. The testing temperature was maintained at 70 °C by submerging the sample holders in an acrylic tank filled with circulated water from an external water bath (Alpha A 6, LAUDA, Lauda-Königshofen, Germany). An initial pre-load of 0.1 N was applied to ensure minimal clearance before the test. Maximum recovery forces were statistically analyzed using the Real Statistics Resource Pack software (Release 8.9.1).[28]

2.6 Corrosion test

The corrosion resistance of the samples in this study was based on the measurement of open-circuit potential (OCP) and linear polarization resistance (LPR). The test was carried out at 70 ± 1 °C using natural spring water (Aura, TIPCO FOODS PCL.) as an electrolyte to mimic the natural geothermal hot spring environment. The compositions of the natural spring water used in this study are shown in Table 1, as provided by the manufacturer. The three-electrode cell was assembled using Pt counter electrode, Ag/AgCl reference electrode, and sample as the working electrode. OCP was measured for 3,600 seconds, followed by LPR measurement from -600 to 1,600 mV vs Ag/AgCl using a potentiostat (Metrohm drop sets, µStat-i 400) at 20 mV/min, with a scanning range.[29] The obtained data were analyzed using the 'manufacturer's software.

Table 1. Nominal chemical composition of natural spring mineral water.

Nominal Chemical Composition	mg/L
Silica	50
Calcium	57
Potassium	1.5
Magnesium	6.5
Bicarbonate	220
Chloride	<1
Fluoride	0.39
Sulphate	6
Sodium	4
pH	7.6

2.7 Offset crankshaft SMA heat engine mechanism

The mechanism used for the pilot study was adapted and modified from the previous work, which was the offset crankshaft.[26] The outer and inner wheel diameters were 400 and 63 mm, respectively. The widths of wheels were 310 mm for the outer wheel and 210 mm for the inner. Two wheels were connected via 8 rows of SMA actuators, each containing 13 springs with 20 mm spacing. The rows were located along the surface of the outer wheel at 27.3° and of the inner wheel at 8.3° from the longitudinal axis of the wheel. The distance between rows was 225 mm and 112 mm on the outer and inner wheels, respectively. Other relevant dimensions are shown in Figs. 1(a) and 1(b). It is noted that the SMA springs used in this pilot study were annealed at 350 °C for 60 minutes without subsequent etching.

The pilot study was conducted at the nominal water temperature of 70 °C, and the actual temperature was monitored using digital thermocouples with an accuracy of ±1 °C. The torque generated by the engine was measured using an advanced force and torque indicator (AFTI, Mecmesin) equipped with a rotary torque sensor (Model 2100-175, NCTE) and variable dead weight (Koshin Seikosho PERMA-TORK HC4-4J Brake Clutch) attached to the shaft of the engine, as shown in Fig. 1(c). In addition, a digital timer and a manual revolution counter were used to determine the average rotational speed, which was also required to determine the mechanical output power of this engine as power equals torque multiplied by rotational speed.[26] On the other hand, the overall efficiency of the engine was calculated by dividing the calculated mechanical work (W_{out}) by the heat required for the

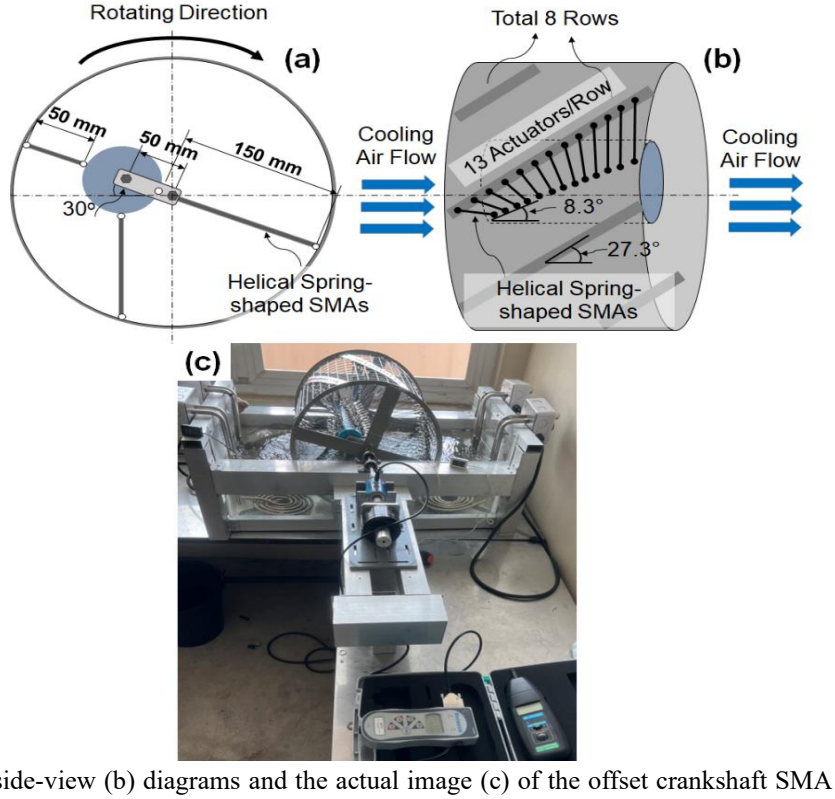

Fig. 1 Front-view (a) and side-view (b) diagrams and the actual image (c) of the offset crankshaft SMA heat engine used for pilot study.

austenitic transformation of the SMAs (Q_{in}) analyzed from the DSC curve, assuming that the SMAs have uniformly undergone complete martensite-to-austenite transformation in each cycle.[26,30-32] The apparent Q_{in} per cycle calculated in this study was 1,019 J using 104 SMA spring actuators with an average spring mass of 1.8 g per spring.

3. Results

3.1 Surface characterization

Images of the surfaces of SMA samples annealed at 350 °C for 30 and 60 min with and without etching are shown in Fig. 2, from which the significant differences were not visually noticeable. On the other hand, surface profiles from each sample were also measured and shown in Fig. 3. The etched samples' surfaces were noticeably coarser than those of no-etching samples.

The surfaces of the samples were further characterized in terms of their cross-sectional appearance and chemical composition using SEM-EDS line scan, of which the relative data are shown in Figs. 4 and 5, respectively. In addition to Ti, Ni, and Cu, it could be seen that the O content was relatively higher on the surface of no-etching samples (Figs. 5(a) and 5(c)) than those of etched (Figs. 5(b) and 5(d)), particularly at the outer surface. The difference was more evident in the sample annealed for 60 min. Furthermore, it could also be observed that the oxide thickness was approximately 1 µm for 30-min annealed samples and 1.5 µm for 60-min.

3.2 Phase transformation

Phase transformation temperatures of the samples were determined by DSC. Exothermic and endothermic changes in the heat flow across the samples within the temperature ranging between 0 °C and 100 °C are shown in Fig. 6 The endothermic changes in the heat flow during the heating cycle corresponded to the structural transformation from B19' monoclinic to B2 cubic, whereas the exothermic changes in the cooling cycle were corresponding to the transformation from B2 to B19'. It could be noted that neither endothermic nor exothermic changes in heat flow were observed in the as-drawn samples. Furthermore, the presence of intermediate R-phase was also noticeable from double peaks of the DSC curve obtained from the no-etching sample annealed for 60 min.[33] The transformation temperatures were also quantified and presented in Table 2.

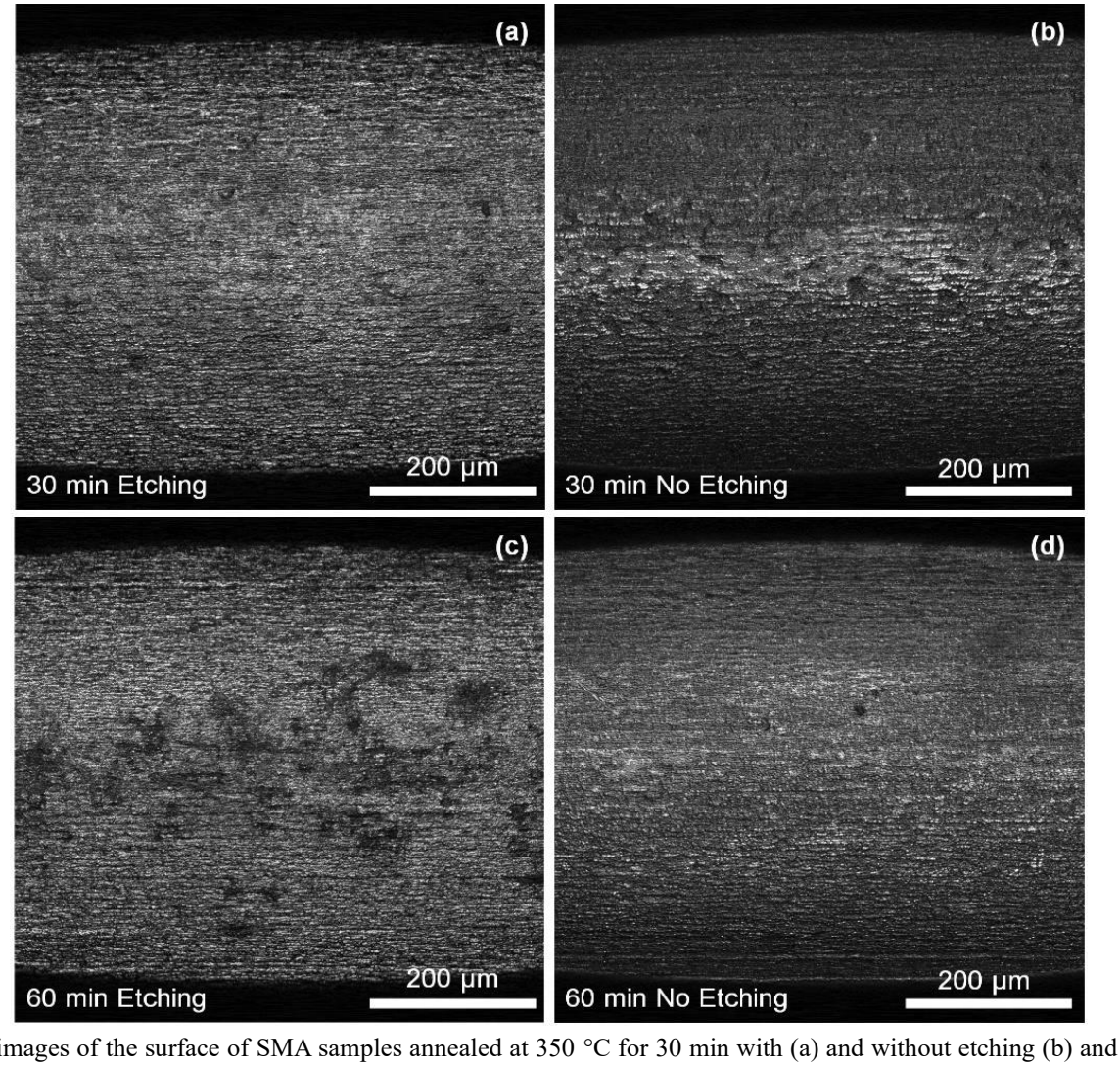

Fig. 2 Laser images of the surface of SMA samples annealed at 350 °C for 30 min with (a) and without etching (b) and for 60 min with (c) and without etching (d) at 20X magnification.

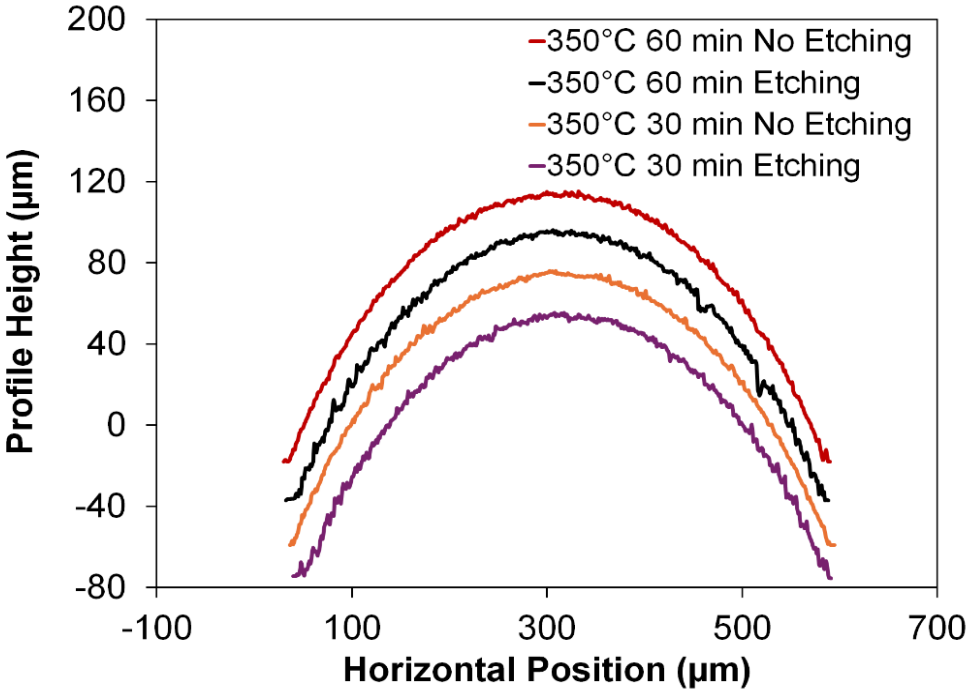

Fig. 3 Surface profiles of the SMA samples annealed at 350 °C for 30 and 60 min with and without etching.

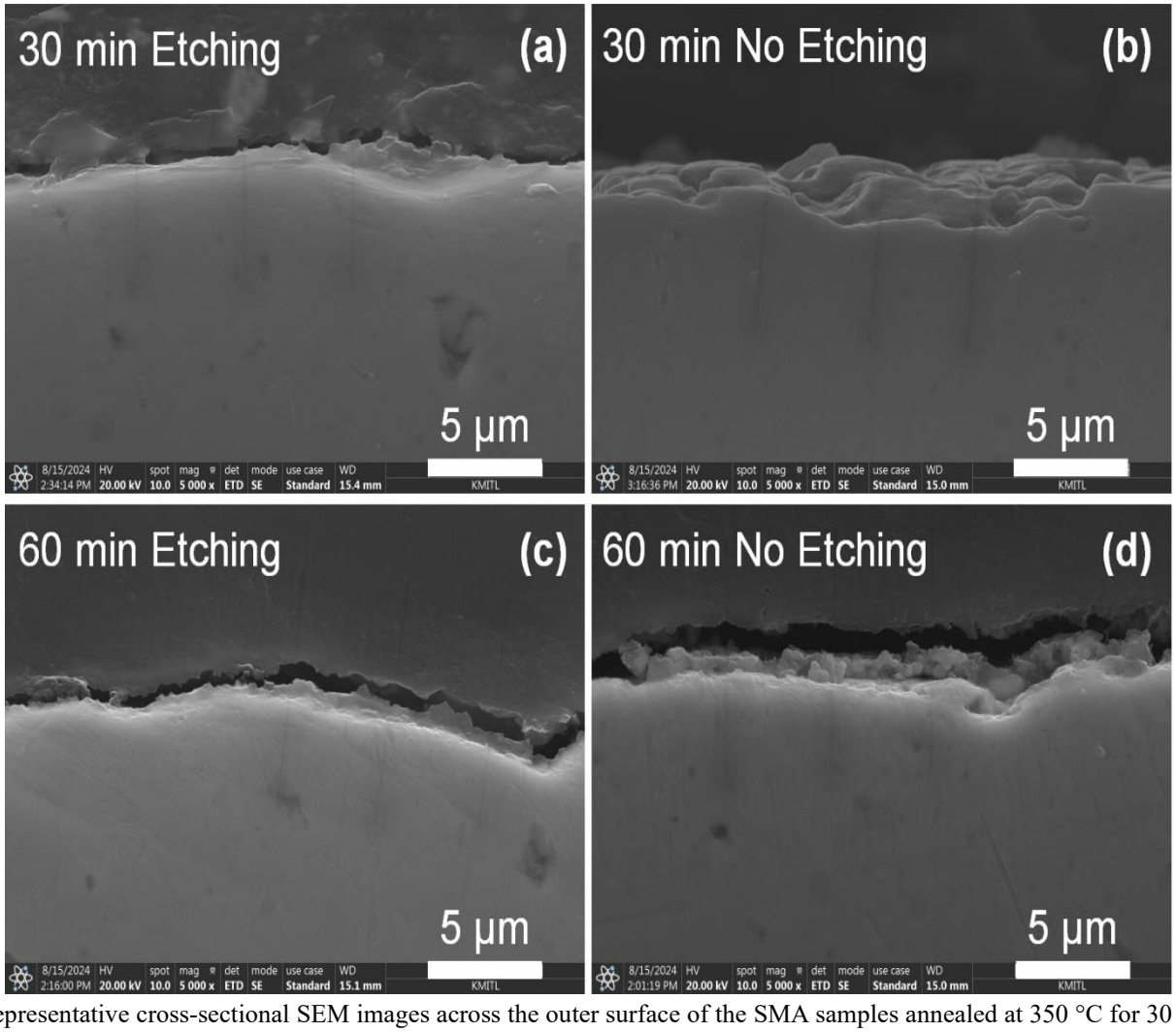

Fig. 4 Representative cross-sectional SEM images across the outer surface of the SMA samples annealed at 350 °C for 30 min with (a) and without etching (b) and for 60 min with (c) and without etching (d) at 5,000X magnification.

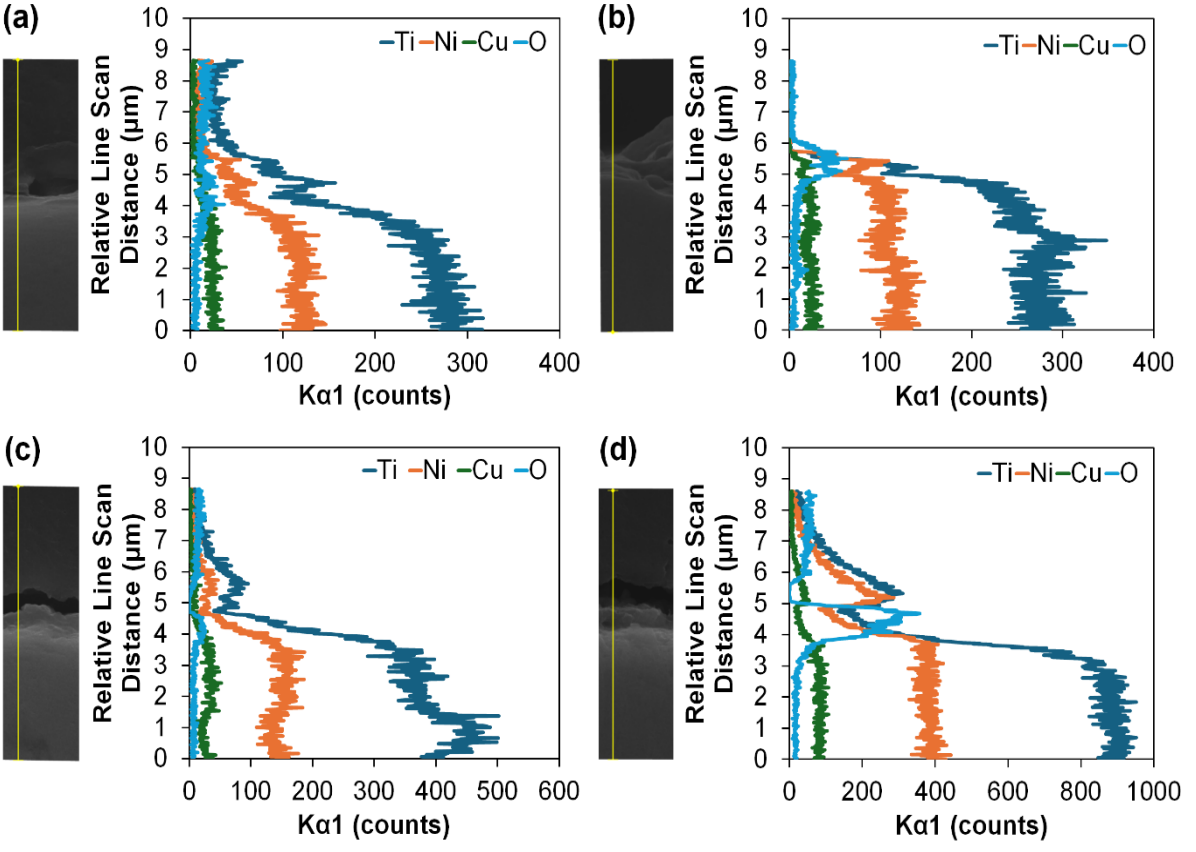

Fig. 5 Relative chemical composition across the depth from the outer surface of the SMA samples annealed at 350 °C for 30 min with (a) and without etching (b) and for 60 min with (c) and without etching (d).

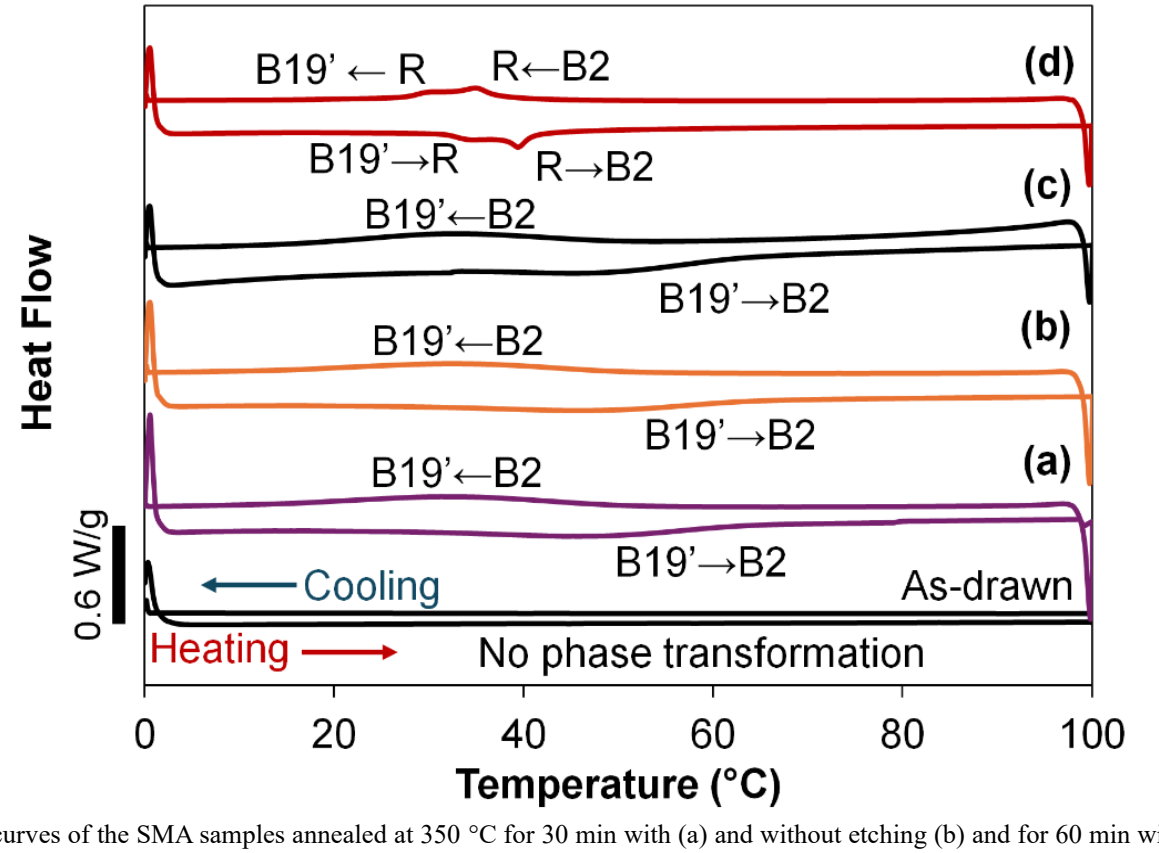

Fig. 6 DSC curves of the SMA samples annealed at 350 °C for 30 min with (a) and without etching (b) and for 60 min with (c) and without etching (d).

Table 2. Quantified transformation temperature of the SMA samples from DSC curves.

Samples	Transformation Temperature (°C)					
	M_s	M_f	R_s	R_f	A_s	A_f
350°C 30 min Etching	52.0	13.5	-	-	25.5	63.5
350°C 30 min No Etching	52.5	14.3	-	-	25.0	62.3
350°C 60 min Etching	52.0	15.8	-	-	33.0	64.3
350°C 60 min No Etching	31.5	27.5	38.0	32.5	38.3	41.5

M_s = Martensite start temperature
M_f = Martensite finish temperature
R_s = Rhombohedral start temperature
R_f = Rhombohedral finish temperature
A_s = Austenite start temperature
A_f = Austenite finish temperature

It is understood that the optimal operating temperature of the SMA samples would be higher than their A_f at the heating side and lower than their M_s at the cooling side, which were over 64.3 °C and below 52.0 °C, respectively, for the samples in this study. Moreover, it was found from the results that etching does not significantly affect the transformation temperatures of the samples annealed for 30 min. On the other hand, the etching effect was significant in the samples annealed for 60 min as the presence of R-phase was suppressed after the etching process. Moreover, the presence of R-phase has significantly reduced A_f to 41.5 °C and M_s to 31.5 °C.

3.3 Recovery force measurement

Figure 7 shows the measured recovery force and displacement from the SMA spring samples at 70 °C, which is higher than A_f temperature of all samples. The result shows that the influence of etching was not significant when annealing the samples for 30 min, with the average maximum recovery force of 6.05 N and 6.28 N for etched and unetched samples at 70-mm displacement, respectively. On the other hand, the difference was significant in the samples annealed for 60 min. The average maximum recovery force of etched and unetched samples was 7.35 N and 8.32 N, respectively. Moreover, it could also be noticed that the longer annealing time could also result in a significant increase in the average maximum recovery force, as shown in the figure. In addition, the values of measured maximum recovery forces used for ANOVA analysis are tabulated in Table 3.

Table 3. The measured maximum recovery forces used for ANOVA analyses.

Samples	Measured Maximum Recovery Force (N)				
	Sample 1	Sample 2	Sample 3	Mean	SD
350°C 30 min Etching	6.182	5.988	5.988	6.053	0.112
350°C 30 min No Etching	6.466	6.033	6.331	6.276	0.222
350°C 60 min Etching	7.899	7.272	6.884	7.352	0.512
350°C 60 min No Etching	8.019	8.467	8.481	8.322	0.263

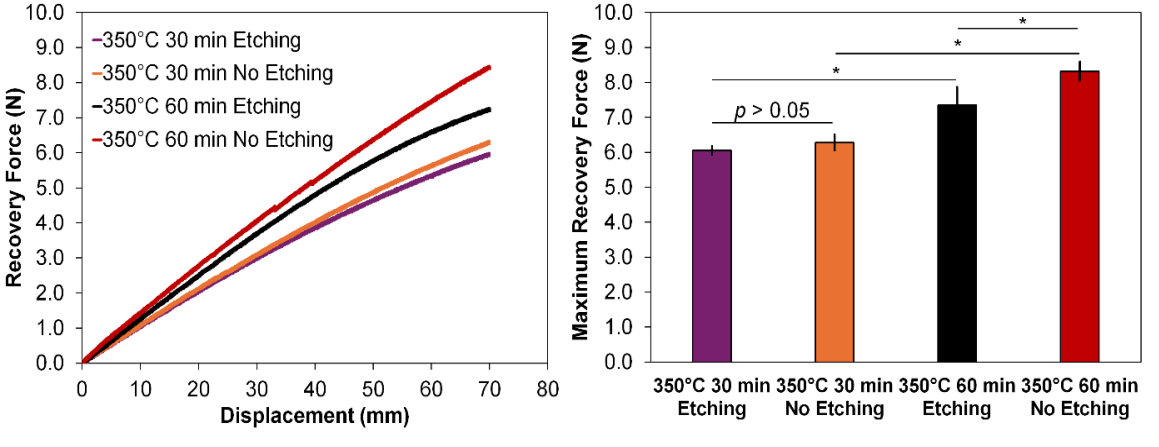

Fig. 7 Representative recovery force within 70-mm displacement (left) and the average maximum recovery force (right) measured from the SMA spring samples at 70 °C. Error bars represent SD (n = 3). * represents $p < 0.05$ (One-way ANOVA with 'Tukey's HSD pairwise comparison).

3.4 Corrosion test

The measured open-circuit potentials (OCPs) and linear polarization resistance (LPR) curves are shown in Fig. 8. It was observed from the results that the OCP of the samples annealed for 30 min were stabilizing towards 0.0075 V and 0.0594 V for etched and unetched condition, respectively. On the other hand, the OCPs were 0.0156 V and 0.0642 V for etched and unetched samples annealed for 60 min, respectively. It could be seen that etching and the increased annealing time could result in the lower OCP. Moreover, the LPR curves have demonstrated that passivation occurred in etched samples and was not observable from the unetched samples. The LPR data were then fitted to obtain E_{corr} and I_{corr}, as shown in Table 4. The results showed that the etched samples tend to exhibit lower E_{corr} than the unetched samples from similar annealing conditions. However, I_{corr} was also found to have a similar trend.

Table 4. Fitted E_{corr} and I_{corr} from the linear polarization curves of the SMA samples.

	E_{corr} (V)	I_{corr} (μA/cm^2)
30 min Etching	-0.046	0.053
30 min No Etching	-0.040	0.311
60 min Etching	-0.038	0.132
60 min No Etching	-0.031	0.239

3.5 Performance of the pilot offset crankshaft SMA heat engine

Due to the promising properties, the unetched samples annealed for 60 min were used as actuators for the pilot offset crankshaft SMA heat engine test. Torque and rotational speed were measured when submerging the engine in water at 70 °C. The measured data were then used to calculate mechanical power and efficiency. The results are shown in Fig. 9. It can be seen that the engine could successfully convert thermal energy into mechanical work with the maximum torque and power of 4.75 N·m and 2.512 W, respectively. On the other hand, the maximum efficiency of this pilot engine was at 0.99%, and the rotational speed could be as high as 31 rpm.

4. Discussion

4.1 Surface properties of the SMA samples

Chemical etching is one of the common techniques for modifying the surfaces of metallic samples to meet various engineering requirements, such as sample preparation for optical microstructure analysis, and aesthetic requirements, such as surface decontamination from oxide layer or other contaminants. It could be seen from the results that etching has interacted with the surfaces of SMA samples, resulting in changes in the surface roughness and the oxygen content. Although the changes in the surface roughness may not be evident, the reduced oxygen content in the surface indicates that the oxide layer was removed by etching and thus the influence of oxide film can be discussed by comparing etched and unetched samples.

In general, oxide films are formed on the surface of Ti-based SMAs via oxidation, which could be induced by heat treatment. This is generally not a concern for alloy processing as it could protect the alloy from corrosion. However, it was also suggested that excessive oxide formation could affect the alloys' structural transformation and mechanical properties.[34] Since the oxide is a brittle ceramic phase that does not exhibit shape memory effect, it could hinder the phase transformation and performance of the alloys. In this study, heat treatment at 350 °C was used to induce shape memory of the TiNiCu alloys into the helical spring shape, which was lower than the temperature used in previous oxidation studies on the TiNi.[21-24] Therefore, it could be expected that only thin layers of oxides would be formed on the samples as indicated by the

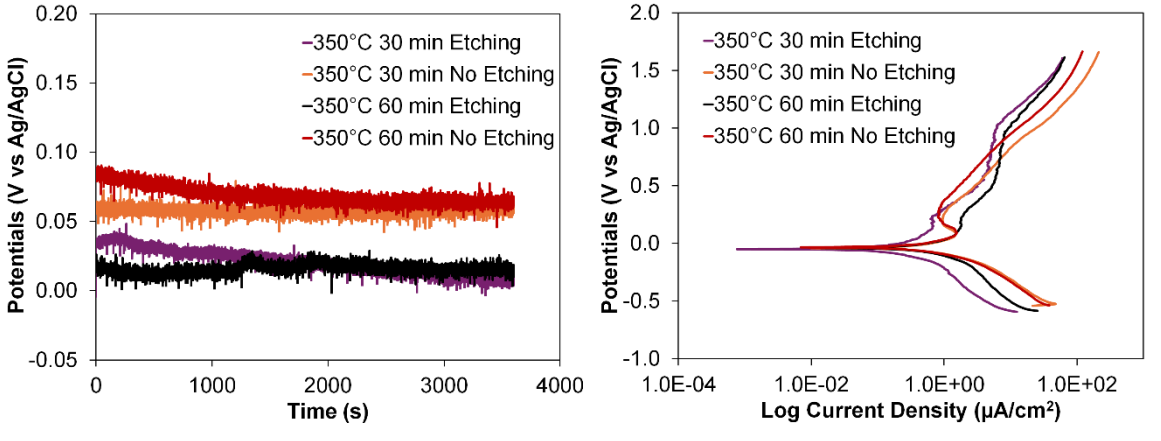

Fig. 8 The open-circuit potentials (left) and linear polarization resistance curves (right) of the SMA samples submerged in natural spring water at 70 °C.

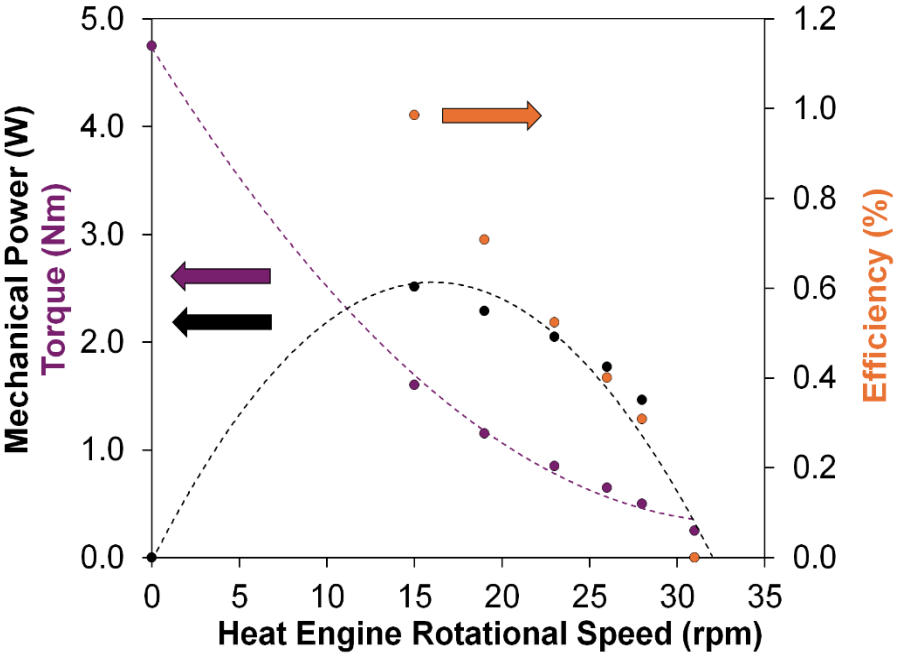

Fig. 9 Torque, mechanical power, and efficiency of the pilot offset crankshaft SMA heat engine using the unetched samples annealed for 60 min.

SEM-EDS line scan, and the thickness could increase with prolonged treatment time.[16,35] Furthermore, the composition of the oxide formed is expected to be TiO_2 as it is widely understood that Ti oxidizes relatively easier than other elements in the alloys used in this study, including Ni and Cu, with possible Ti-Ni intermetallic layer being formed underneath.[21-24,35,36] Although the chemical composition from the EDS line scan is consistent with the previous study, this study discusses the influence of the oxide layer collectively and may require further characterization to identify its exact composition.[21]

4.2 Phase transformation and recovery force of the SMA samples

During the operation as the heat engine actuator, the microstructure of Ti-based SMAs could be in three different phases: B2 cubic austenite, B19' monoclinic martensite; and, occasionally, rhombohedral phase (R-phase).[37] Based on the results from DSC, it could be seen that the effect of oxide films on transformation temperature was not evident in the sample annealed for 30 min; however, it became evident when annealing the samples for 60 min as phase transformation to R-phase was not visible after etching. This could be because oxide formation was not sufficiently formed to affect the alloy properties. It is also noted that the forward transformation temperatures to austenite and backward transformation temperatures of each sample are different due to thermal hysteresis from lattice distortion.

The R-phase exhibits a structure similar to B19' (monoclinic structure) and has a rhombohedral structure with limited flexibility.[38] The presence of R-phase is reported to be common in aged TiNiCu alloys, and this could be beneficial for use as a heat engine actuator as R-phase transformation exhibits smaller thermal hysteresis (approximately 5 °C) and less lattice distortion than martensitic transformation.[34] In addition to the oxide, the R-phase transformation could also be induced by other alloy processing methods, such as precipitation, thermal cycling, and the introduction of a third element.[39,40] Furthermore, it could be noticed that the increased annealing time could increase A_s transformation temperature, particularly in etched samples. This observation could be due to the strengthening effect within the internal structure, including the formation of small precipitates. As a result, it would require higher energy to transform the matrix structure, resulting in a higher as transformation temperature.[41]

In terms of the heat engine application, the alloys would operate at above their A_f temperature on one side and lower than their M_s temperature on the other side of the engine in order to induce force and displacement through the cycles of austenitic-martensitic transformation, known as shape memory effect. In order to characterize the recovery force of the SMA samples, this study has carried out a test using a modified universal tensile testing machine to measure the force generated by the samples at 70 °C, which is above A_f of all test samples. It could be noticed from the results that, despite comparable A_f temperatures, the etched samples without the presence of R-phase exhibited significantly different maximum recovery force, and it is directly proportional to the annealing time. This observation implies that the stability of the austenite phase could direct the level of force generated by the SMA actuator. Furthermore, when

comparing with unetched samples, it is noticeable that the influence of the oxide films on the recovery force was not significant in the samples annealed for 30 min.

On the other hand, the difference became significant in the samples annealed for 60 min, partly due to the presence of R-phase transformation. These findings are consistent with the DSC data, suggesting that the formation of oxide was insufficient for affecting samples' properties with 30-min annealing. Moreover, it would also be worth pointing out that annealing longer than 60 minutes may potentially affect the properties of the SMAs as the alloy compositions could significantly change from diffusion during the oxide formation, such as stress-induced martensite and shape memory effects.[21-24]

4.3 Corrosion resistance and feasibility of heat engine application

Corrosion is one of the concerns when operating metallic engineering parts in humidified environments, including the use of heat engines to harvest geothermal energy from hot springs. Therefore, this study has investigated the corrosion resistance of the SMAs in natural spring water. The results indicate that the etched samples tend to have lower OCP than unetched, suggesting that they are more reactive to oxidative reactions.[42] This observation highlights the role of oxide films in preventing metal corrosion, which has already been widely noted, and this application is no different. Furthermore, the LPR curves have also shown consistent trends with the OCP data, from which the etched samples have exhibited lower E_{corr}. This observation implies that the samples without oxide films tend to have lower stability in the oxidative environment, indicating lower corrosion resistance. The passivation characteristics were observed from the etched samples, which indicates the formation of new protective films.[43,44] The formed passive film was primarily composed of TiO_2, which is commonly observed in Ti alloys.[45] By comparing the data between etched and unetched samples, it is understood that the presence of oxide films on the alloy surface could enhance corrosion resistance.[46] However, it is worth pointing out the difference in I_{corr} between etched and unetched samples. In theory, I_{corr} indicates the rate of electrochemical reactions, which is directly proportional to the corrosion rate.[47] Despite the lower E_{corr}, the etched samples also exhibited lower I_{corr} than the etched samples, indicating the slower corrosion rate than the unetched samples. This could be interpreted that, although the etched sample is more likely to undergo oxidative reactions, it could form passive film *in situ* that slows down the reactions.[47] On the contrary, the unetched samples with oxide film presented are less likely to undergo oxidative reactions, but once the corrosion occurs, the rate could be high. Therefore, it is worth noting that long-term surface stability could also be another point to consider when designing the SMA actuator for heat engine applications, alongside other properties. In addition, it could also be noticed that the unetched samples annealed for 60 min exhibited greater corrosion resistance than 30 min. This could be because the longer annealing time has resulted in higher structural stability, which is reflected by greater corrosion resistance.[46]

Based on the results, it could be decided that the unetched samples annealed for 60 min provide the lowest A_f transformation temperature, the highest recovery force, and high corrosion resistance. Therefore, this condition was selected for a pilot test for heat engine application, and it was shown to be capable of driving the offset crankshaft heat engine to convert thermal energy into mechanical work at 70 °C. It is observed from the results that the engine could operate at a wide range of rotational speed and torque, which delivers various power and efficiency. This information can be used to couple the engine with a suitable generator for optimal power generation in the future. Although it has been shown earlier that the performance of the engine was dependent on the geometry and water temperature, this study suggests another factor that could be used for engine optimization, which is the oxide formed on the surface of the SMA actuators.[26] Despite a similar trend, it may not be appropriate to compare the performance of the pilot engine in this study with the previous one due to the difference in engine geometry, and it could be expected that the performance of this engine could improve with increasing water temperature.[26] Nonetheless, this study has confirmed that etching may not be necessary during the alloy processing; however, the optimal oxide condition could still be inconclusive as it could affect the fatigue behavior of the alloys.[14] Therefore, it would be of interest to future studies to investigate the influence of the oxide films on the fatigue properties of the SMA actuators used for heat engine application.

5. Conclusions

It could be concluded from this study that oxide films formed on the surface of SMAs are beneficial for use as heat engine actuators due to the following reasons. Firstly, the oxide could influence R-phase transformation, lowering A_f transformation and increasing the force generated from the shape memory effect. Secondly, the oxide works as a protective layer to prevent SMAs from corrosion when using heat engine to harvest the energy from geothermal hot springs. Heat-treated samples at 350°C for 60 min without etching were the most suitable for using as heat engine actuator for harvesting geothermal energy from hot springs. However, further study may be required to investigate the influence of oxide films on the fatigue properties of the SMAs, which could dictate the heat engine's durability.

Acknowledgments

This work was financially supported by Rajamangala University of Technology Krungthep (RMUTK Research Grant, FY 2023).

Conflict of Interest

There is no conflict of interest.

Supporting Information

Not applicable.

References

[1] A. I. Osman, L. Chen, M. Yang, G. Msigwa, M. Farghali, S. Fawzy, D. W. Rooney, P.-S. Yap, Cost, environmental impact, and resilience of renewable energyunder a changing climate: a review, *Environmental Chemistry Letters*, 2023, **21**, 741-764, doi: 10.1007/s10311-022-01532-8.

[2] S. Ghoddousi, B. Rezaie, S. Ghandehariun, Guideline for electricity generation from hot springs (natural energy storage systems): a techno-enviro-economic assessment, *Sustainable Energy Technologies and Assessments*, 2021, **47**, 101407, doi: 10.1016/j.seta.2021.101407.

[3] R. A. Kishore, S. Priya, A Review on low-grade thermal energy harvesting: materials, methods and devices, *Materials*, 2018, **11**, 1433, doi: 10.3390/ma11081433.

[4] A. V. Herzog, T. E. Lipman, J. L. Edwards, D. M. Kammen, Renewable energy: a viable choice, *Environment: Science and Policy for Sustainable Development*, 2001, **43**, 8-20, doi: 10.1080/00139150109605150.

[5] T. Sakuma, U. Iwata, Working characteristics of a reciprocating-type heat engine using shape memory alloys, *JSME International Journal Series B Fluids and Thermal Engineering*, 1998, **41**, 344-350, doi: 10.1299/jsmeb.41.344.

[6] G. Oluleye, M. Jobson, R. Smith, S. J. Perry, Evaluating the potential of process sites for waste heat recovery, *Applied Energy*, 2016, **161**, 627-646, doi: 10.1016/j.apenergy.2015.07.011.

[7] M. Langan, K. O'Toole, A new technology for cost effective low grade waste heat recovery, *Energy Procedia*, 2017, **123**, 188-195, doi: 10.1016/j.egypro.2017.07.261.

[8] A. L. Browne, P. W. Alexander, N. Mankame, P. Usoro, N. L. Johnson, J. Aase, P. Sarosi, A. C. Keefe, G. P. McKnight, G. Herrera, C. Churchill, J. Shaw, J. Brown, International Workshop: Smart Materials, Structures & NDT in Aerospace, Montreal Canada, 2011.

[9] R. A. Abubakar, F. Wang, L. Wang, A review on Nitinol shape memory alloy heat engines, *Smart Materials Structures*, 2021, **30**, 013001, doi: 10.1088/1361-665X/abc6b8.

[10] J. M. Jani, M. Leary, A. Subic, M. A. Gibson, A review of shape memory alloy research, applications and opportunities, *Materials & Design*, 2014, **56**, 1078-1113, doi: 10.1016/j.matdes.2013.11.084.

[11], A. Riccio, A. Sellitto, D. Borrelli, S. H. T. V. R. S. N. Italy, R. Sansone, S. H. T. V. R. S. N. Italy, A. Caraviello, S. H. T. V. R. S. N. Italy, U. Riccio, A. Torluccio, L. Pacini, R. Mohr, On the development of a passive shape memory alloy- based cooling system–part I: design and implementation, *Engineered Science*, 2023, **25**, 927, doi: 10.30919/es927.

[12] Z. Han, Y. Niu, X. Shi, D. Pan, H. Liu, H. Qiu, W. Chen, B. B. Xu, Z. M. El-Bahy, H. Hou, E. R. Elsharkawy, M. A. Amin, C. Liu, Z. Guo, MXene@c-MWCNT Adhesive Silica Nanofiber Membranes Enhancing Electromagnetic Interference Shielding and Thermal Insulation Performance in Extreme Environments, *Nano-Micro Letters*, 2024, **16**, 195, doi: 10.1007/s40820-024-01398-1.

[13] A. Riccio, A. Sellitto, A. Caraviello, S. H. T. V. R. S. N. Italy, U. Riccio, A. Torluccio, L. Pacini, R. Mohr, On the development of a passive shape memory alloy- based cooling system–part II: design justification, *Engineered Science*, 2023, **25**, 928, doi: 10.30919/es928.

[14] O. W. Bertacchini, D. C. Lagoudas, E. Patoor, Thermomechanical transformation fatigue of TiNiCu SMA actuators under a corrosive environment–Part I: Experimental results, *International Journal of Fatigue*, 2009, **31**, 1571-1578, doi: 10.1016/j.ijfatigue.2009.04.012.

[15] J. Zhu, H. H. Wu, Y. Wu, H. Wang, T. Zhang, H. Xiao, Y. Wang, S. O. Shi, Influence of Ni_4Ti_3 precipitation on martensitic transformations in NiTi shape memory alloy: R phase transformation, *Acta Materialia*, 2021, **207**, 116665, doi: 10.1016/j.actamat.2021.116665.

[16] G. S. Firstov, R. G. Vitchev, H. Kumar, B. Blanpain, J. Van Humbeeck, Surface oxidation of NiTi shape memory alloy, *Biomaterials*, 2002, **23**, 4863-4871, doi: 10.1016/s0142-9612(02)00244-2.

[17] C. L. Chu, S. K. Wu, Y. C. Yen, Oxidation behavior of equiatomic TiNi alloy in high temperature air environment, *Materials Science and Engineering: A*, 1996, **216**, 193-200, doi: 10.1016/0921-5093(96)10409-3.

[18] C. H. Xu, X. Q. Ma, S. Q. Shi, C. H. Woo, Oxidation behavior of TiNi shape memory alloy at 450–750°C, *Materials Science and Engineering: A*, 2004, **371**, 45-50, doi: 10.1016/s0921-5093(03)00287-9.

[19] J. Huang, P. Dong, W. Hao, T. Wang, Y. Xia, G. Da, Y. Fan, Biocompatibility of TiO_2 and TiO_2/heparin coatings on NiTi alloy, *Applied Surface Science*, 2014, **313**, 172-182, doi: 10.1016/j.apsusc.2014.05.182.

[20] D. P. Aun, M. Houmard, M. Mermoux, L. Latu-Romain, J. C. Joud, G. Berthom'e, V. T. L. Buono, Development of a flexible nanocomposite TiO_2 film as a protective coating for bioapplications of superelastic NiTi alloys, *Applied Surface Science*, 2016, **375**, 42-49, doi: 10.1016/j.apsusc.2016.03.064.

[21] A. Mahmud, Z. Wu, J. Zhang, Y. Liu, H. Yang, Surface oxidation of NiTi and its effects on thermal and mechanical properties, *Intermetallics*, 2018, **103**, 52-62, doi: 10.1016/j.intermet.2018.09.013.

[22] Z. Wu, A. Mahmud, J. Zhang, Y. Liu, H. Yang, Surface oxidation of NiTi during thermal exposure in flowing argon environment, *Materials & Design*, 2018, **140**, 123-133, doi: 10.1016/j.matdes.2017.11.061.

[23] C.W. Ng, A. S. Mahmud, Effect of surface oxidation on thermomechanical behavior of NiTi shape memory alloy wire, *AIP Conference Proceedings*, 2017, **1901**, 120002, doi: 10.1063/1.5010552.

[24] A. S. Mahmud, C. W. Ng, M. F. Razali, Effect of surface oxidation on shape memory behaviour of NiTi alloy, *AIP*

Conference Proceedings, 2016, **1774**, 060006, doi: 10.1063/1.4965114.
[25] S. Khanna, P. Marathey, Utsav, R. Patel, S. Paneliya, R. Chaudhari, J. Vora, A. Ray, R. Banerjee, I. Mukhopadhyay, Unravelling camphor mediated synthesis of TiO_2 nanorods over shape memory alloy for efficient energy harvesting, *Applied Surface Science*, 2021, **541**, 148489, doi: 10.1016/j.apsusc.2020.148489.
[26] K. Srirussamee, A. Khantachawana, B. Hok, A. Phukaoluan, Thermomechanical performance of the offset crankshaft heat engine driven by TiNiCu shape memory alloys, *Engineering Journal*, 2021, **25**, 85-93, doi: 10.4186/ej.2021.25.2.85.
[27] M. Salmerón Sánchez, V. B. Mathot, G. Vanden Poel, J. L. Gómez Ribelles, Effect of the cooling rate on the nucleation kinetics of poly (L-lactic acid) and its influence on morphology, *Macromolecules*, 2007, **40**, 7989-7997, doi: 10.1021/ma0712706.
[28] V. M. Expósito-Suárez, J. A. Suárez-Navarro, P. Vacas-Arquero, A. Caro,. Application of gamma spectrometry for the characterization and influence of the archeological works of an archaeological site, *Journal of Radioanalytical and Nuclear Chemistry*, 2023, **332**, 95-104, doi: 10.1007/s10967-022-08708-0.
[29] A. Phukaoluan, A. Khantachawana, P. Kaewtatip, S. Dechkunakorn, Assessment of corrosion behavior in artificial saliva of wires for orthodontic applications, *Materials Science Forum*, 2018, **917**, 197-201, doi: 10.4028/www.scientific.net/MSF.917.197.
[30] A. Phukaoluan, S. Dum, A. Khantachawana, Influence of Offset Distance and Extension Ratio of Shape Memory Alloys Spring on Mechanical and Electrical Power of Offset Crank Heat Engine, The 14th National Conference on Technical Education and The 9th International Conference on Technical Education, 2022.
[31] J. A. Shaw, C. B. Churchill, M. A. Iadicola, Tips and tricks for characterizing shape memory alloy wire: part 1-differential scanning calorimetry and basic phenomena, *Experimental Techniques*, 2008, **32**, 55-62, doi: 10.1111/j.1747-1567.2008.00410.x.
[32] W. S. Rasband, ImageJ (1.52a) U.S. National Institutes of Health, Bethesda, Maryland USA, 2018.
[33] M. Pohl, T. Glogowski, S. Kühn, C. Hessing, F. Unterumsberger, Formation of titanium oxide coatings on NiTi shape memory alloys by selective oxidation, *Materials Science and Engineering: A*, 2008, **481**, 123-126, doi: 10.1016/j.msea.2007.02.151.
[34] M. Tabesh, K. C. Atli, J. Rohmer, B. E. Franco, I. Karaman, J. G. Boyd, D. C. Lagoudas, Design of shape memory alloy pipe couplers: Modeling and experiments, *Proceedings of SPIE*, 2012, **8343**, 141-185, doi: 10.1117/12.915361.
[35] G. Fan, W. Chen, S. Yang, J. Zhu, X. Ren, K. Otsuka, Origin of abnormal multi-stage martensitic transformation behavior in aged Ni-rich Ti–Ni shape memory alloys, *Acta Materialia*, 2004, **52**, 4351-4362, 10.1016/j.actamat.2004.06.002.
[36] C.-M. Chan, S. Trigwell, T. Duerig, Oxidation of an NiTi alloy, *Surface and Interface Analysis*, 1990, **15**, 349-354, doi: 10.1002/sia.740150602.
[37] K. Otsuka, C.W. Wayman, Shape Memory Materials, Cambridge University Press, Cambridge, 1998.
[38] H. C. Ling, K. Roy, Stress-induced shape changes and shape memory in the R and martensite transformations in equiatomic NiTi, *Metallurgical Transactions A*, 1981, **12**, 2101-2111, doi: 10.1007/bf02644180.
[39] S. H. Chang, S. K. Wu, Effect of cooling rate on transformation temperature measurements of Ti50Ni50 alloy by differential scanning calorimetry and dynamic mechanical analysis, *Materials Characterization*, 2008, **59**, 987-990, doi: 10.1016/j.matchar.2007.08.014.
[40] Y. Zheng, F. Jiang, L. Li, H. Yang, Y. Liu, Effect of ageing treatment on the transformation behaviour of Ti–50.9 at.% Ni alloy, *Acta Materialia*, 2008, **56**, 736-745, doi: 10.1016/j.actamat.2007.10.020.
[41] T. Fukuda, M. Kitayama, T. Kakeshita, T. Saburi, Martensitic Transformation behavior of a shape memory Ti–40.5Ni–10Cu Alloy Affected by the C11b-type precipitates, *Materials Transactions JIM*, 2014, **37**, 1540-1546, doi: 10.2320/matertrans1989.37.1540.
[42] Y. Feng, Z Du, Z. Hu, Effect of Ni addition on the corrosion resistance of NiTi alloy coatings on AISI 316L substrate prepared by laser cladding, *Coatings*, 2021, **11**, 1139, doi: 10.3390/coatings11091139.
[43] Y. Hu, Z. Wang, J. Ai, S. Bu, H. Liu, Preparation of coating on the titanium surface by micro-arc oxidation to improve corrosion resistance, *Coatings*, 2021, **11**, 230, doi: 10.3390/coatings11020230.
[44] A. Phukaoluan, A. Khantachawana, S. Dechkunakorn, N. Anuwongnukroh, P. Santiwong, J. Kajornchaiyakul, Effect of Cu and Co addition on corrosion behavior of NiTi alloys for orthodontic application, *Advanced Materials Research*, 2012, **378**, 650-654, doi: 10.4028378-379.650.
[45] A. W. Hansen, L. V. Rossa Beltrami, L. M. Antonini, D. J. Villarinho, J. C. Klein das Neves, C. E. Bruno Marino, C. F. Malfatti, Oxide formation on NiTi surface: influence of the heat treatment time to achieve the shape memory, *Materials Research*, 2015, **18**, 1053-1061, doi: 10.1590/1516-1439.022415.
[46] I. Milošev, B. Kapun, The corrosion resistance of Nitinol alloy in simulated physiological solutions, *Materials Science and Engineering: C*, 2012, **32**, 1087-1096, doi: 10.1016/j.msec.2011.11.007.
[47] X. H. Ye, F. Yu, M. Curioni, Z. Lin, H. J. Zhang, H. W. Zhu, Z. Liu, M. L. Zhong, Corrosion resistance of graphene directly and locally grown on bulk nickel substrate by laser irradiation, *RSC Advances*, 2015, **5**, 35384-35390, doi: 10.1039/c5ra01267h.

